

**Experimental study of precisely selected evaporation chains in the decay of excited  $^{25}\text{Mg}$** 

A. Camaiani,<sup>1,2,\*</sup> G. Casini,<sup>2</sup> L. Morelli,<sup>3,4,5</sup> S. Barlini,<sup>1,2</sup> S. Piantelli,<sup>2</sup> G. Baiocco,<sup>6,7</sup> M. Bini,<sup>1,2</sup> M. Bruno,<sup>4,5</sup> A. Buccola,<sup>1,2</sup> M. Cinausero,<sup>8</sup> M. Cicerchia,<sup>8</sup> M. D'Agostino,<sup>4,5</sup> M. Degelier,<sup>9</sup> D. Fabris,<sup>10</sup> C. Frosin,<sup>1,2</sup> F. Gramegna,<sup>8</sup> F. Gulminelli,<sup>11</sup> G. Mantovani,<sup>8</sup> T. Marchi,<sup>8</sup> A. Olmi,<sup>2</sup> P. Ottanelli,<sup>1,2</sup> G. Pasquali,<sup>1,2</sup> G. Pastore,<sup>1,2</sup> S. Valdré,<sup>2</sup> and G. Verde<sup>12</sup>

<sup>1</sup>*Dipartimento di Fisica, Università di Firenze 50019, Italy*

<sup>2</sup>*INFN, Sezione di Firenze 50019, Italy*

<sup>3</sup>*GANIL, CEA/DSM-CNRS/IN2P3, Boite Postale 5027, F-14076 Caen Cedex, France*

<sup>4</sup>*Dipartimento di Fisica, Università di Bologna 40126, Italy*

<sup>5</sup>*INFN, Sezione di Bologna 40127, Italy*

<sup>6</sup>*Dipartimento di Fisica, Università di Pavia 27100, Italy*

<sup>7</sup>*INFN, Sezione di Pavia 27100, Italy*

<sup>8</sup>*INFN, Laboratori Nazionali di Legnaro 35020, Italy*

<sup>9</sup>*Physics Department, Univeristy of Nevsehir, Science and Art Faculty, Nevsehir 50300, Turkey*

<sup>10</sup>*INFN, Sezione di Padova 35131, Italy*

<sup>11</sup>*LPC (IN2P3-CNRS/Ensicaen et Université), F-14076 Caen cédex, France*

<sup>12</sup>*INFN, Sezione di Catania 95125, Italy*



(Received 12 February 2018; published 17 April 2018)

The reaction  $^{12}\text{C} + ^{13}\text{C}$  at 95 MeV bombarding energy is studied using the GARFIELD + Ring Counter apparatus located at the INFN Laboratori Nazionali di Legnaro. In this paper we want to investigate the de-excitation of  $^{25}\text{Mg}$  aiming both at a new stringent test of the statistical description of nuclear decay and a direct comparison with the decay of the system  $^{24}\text{Mg}$  formed through  $^{12}\text{C} + ^{12}\text{C}$  reactions previously studied. Thanks to the large acceptance of the detector and to its good fragment identification capabilities, we could apply stringent selections on fusion-evaporation events, requiring their completeness in charge. The main decay features of the evaporation residues and of the emitted light particles are overall well described by a pure statistical model; however, as for the case of the previously studied  $^{24}\text{Mg}$ , we observed some deviations in the branching ratios, in particular for those chains involving only the evaporation of  $\alpha$  particles. From this point of view the behavior of the  $^{24}\text{Mg}$  and  $^{25}\text{Mg}$  decay cases appear to be rather similar. An attempt to obtain a full mass balance even without neutron detection is also discussed.

DOI: [10.1103/PhysRevC.97.044607](https://doi.org/10.1103/PhysRevC.97.044607)

## I. INTRODUCTION

Reactions with light nuclei have been extensively studied during the past, even at bombarding energies below 100 MeV [1,2], for several reasons. From the technical point of view events with limited number of light fragments are easier to detect and characterize. On the theoretical side, it is interesting to verify the applicability of statistical concepts to the decay of systems formed by a moderate number of nucleons. Moreover, light nuclei, especially those with  $N = Z$ , manifest in their low-lying structure evident clusterization effects which can still persist, but more loosely, with increasing excitation. Therefore, efforts have been done both theoretically, to describe the nature of these quantum systems (in terms of clusters [3]), and experimentally, to find signatures of the clusterization effects also at relatively high excitations [4–7]. In recent years, the interest in this subject of nuclear physics has been renewed [8] thanks to progressively more sophisticated model approaches and to more comprehensive experiments, aiming at

the complete detection and identification of the various ejecta emerging from the collisions. This allows us to finely select and characterize the excited light nuclei; their characteristics can be studied not only on average, for rough classes of events, but also in a very exclusive way following, for instance, the various decay paths for compound nuclei formed in fusionlike reactions. In this respect, the analysis of correlations among the detected particles is quite illuminating because one can try to reconstruct the intermediate nuclei and their states populated during the de-excitation.

In a more general context, fragment spectroscopy and the particle correlations after nuclear collisions represent powerful tools to study the decay of transient systems possibly formed embedded in a nuclear environment. Whether and how the properties of nuclear resonances and states are modified when fragments are formed and disrupted within a nuclear medium is not well known, and the most typical example concerns the Hoyle states in autoconjugate nuclei. Indeed, various efforts have been done or are in progress in this direction using reactions at various bombarding regimes, from Tandem energies like the one in this paper [9,10] to higher energies [10–16].

\*alberto.camaiani@fi.infn.it

In this work we give a further contribution to the experimental study of light excited systems, following the approach of our previous papers [4,5,10,17]. Typically, the method consists of investigating the various decay paths of compound nuclei formed in fusion reactions, selected as accurately as possible, to evidence deviations from the prediction of pure statistical models, which are based on average phase-space considerations and do not include, in their “standard” implementations, the possibility that the branching ratio toward  $\alpha$  emission might be affected by a possible  $\alpha$ -structure of the parent state. The main focus in our previous works was on the fusion reactions  $^{12}\text{C} + ^{12}\text{C}$ , producing  $^{24}\text{Mg}$  nuclei at  $E^* = 61.4$  MeV excitation energy [4,5]. Although we there verified a quite nice agreement of many decay features with the predictions of a statistical model, we observed some deviations in the channels involving the evaporation of only  $\alpha$  particles. Similar behavior was found for the same compound system but formed through the reaction  $^{14}\text{N} + ^{10}\text{B}$  at the same excitation energy. Such additional finding suggests that the deviations are not (or only partially) due to the  $N = Z$  symmetry of the entrance channel, but pertain to the  $N = Z$  compound nucleus itself [10,17].

Therefore, it was quite straightforward to extend our exploration to neighboring systems produced at comparable excitations again through fusion reactions, but with an additional neutron which breaks the  $N = Z$  symmetry. So this paper reports on the fusion reaction  $^{12}\text{C} + ^{13}\text{C}$  at 95 MeV bombarding energy, forming  $^{25}\text{Mg}$  nuclei at  $E^* = 65.7$  MeV. Specifically, we investigate how the additional neutron affects the decay chains of  $^{25}\text{Mg}$  compound nuclei. This is done by comparing the new results with both the predictions of the statistical model and with the previous experimental results on  $^{24}\text{Mg}$  by our apparatus. The main result of the paper is that the same anomaly observed for  $^{24}\text{Mg}$  persists for  $^{25}\text{Mg}$ . This could be tentatively understood from the fact that the neutron emission is the most exothermic decay for the excited  $^{25}\text{Mg}$  ( $Q_{\text{val}} = +8.98$  MeV) besides the  $\gamma$  emission (not seen by our apparatus), thus the probability to populate an excited  $^{24}\text{Mg}$  starting from a  $^{25}\text{Mg}$  compound is high. However, as we will show in detail, such a first chance neutron emission is far from being the dominant decay channel. Rather, the decay pattern of  $^{25}\text{Mg}$  is shown to closely follow the one from  $^{24}\text{Mg}$ , with the extra neutron being preferentially emitted from the (neutron rich) evaporation residue. In this paper we also present a new analysis technique with the aim of estimating the number of evaporated free neutrons which are not detected by our apparatus.

The paper is organized as follows. In Sec. II the characteristics of the experimental apparatus are briefly summarized. Section III describes the criteria adopted in the analysis to select the experimental sample of fusion events and briefly reminds the models used to describe the fusion-evaporation events; Sec. III A discusses the problem of the background of  $^{12}\text{C}$  reactions in the data on  $^{13}\text{C}$ . The general features of the selected fusion events are presented in Sec. IV where they are compared with the statistical code predictions. The detailed analysis of the various decay chains, the comparison between the data of  $^{25}\text{Mg}$  and  $^{24}\text{Mg}$  and the main findings are discussed in Secs. V, VI, and VII. A summary of the work is given in Sec. VIII.

## II. EXPERIMENTAL APPARATUS

The experimental apparatus consists of the multidetector GARFIELD and Ring Counter, located in the Hall III of Laboratori Nazionali di Legnaro (LNL): a complete description and details can be found elsewhere [18]. Briefly, GARFIELD is a two-stage detector consisting of two identical microstrip gas chambers (the  $\Delta E$  stage) and CsI(Tl) crystals (for residual particle energy). The chambers allow particle identification through  $\Delta E$ - $E$  correlations and pulse shape analysis (PSA) in CsI(Tl). The Ring Counter (hereafter referred to as RCO) is a three-stage hodoscope fully equipped with digital electronics: it is made of an eight-sector ionization chamber (IC), followed by segmented reverse mounted silicon detectors and, as last stage, CsI(Tl) crystals. The RCO covers the polar range from  $7^\circ$  up to  $17^\circ$ , while the GARFIELD geometry covers the angular range from  $30^\circ$  to  $150^\circ$  with 180 CsI(Tl) crystals. Both detectors have a complete azimuthal symmetry. The combination of the two devices allows for a geometrical efficiency of almost 80% of  $4\pi$ , also ensuring a good granularity (around 300 electronic channels). Both GARFIELD and RCO are optimized for the detection of charged fragments with low energy thresholds. The RCO is dedicated to the detection and identification of forward emitted fragments, which in the presently studied case are mainly fragments with  $Z \geq 3$ . They are efficiently identified in charge by the RCO via the  $\Delta E$ - $E$  correlation IC-Si and, only for fragments with  $3 \leq Z \leq 8$ , also using the PSA in the Silicon detectors with an energy threshold approximatively of 1.5 MeV/ $u$ . Light charged particles (LCPs) can be isotopically identified through Si-CsI(Tl) correlation and PSA in CsI(Tl), while  $\alpha$  particles (without mass) are identified also using IC-Si correlations and PSA in Silicon detectors.

On the contrary, GARFIELD ensures the detection of most LCPs, which are spread over a wide angular domain. Monte Carlo simulations showed that almost the 80% of the detected LCPs are detected by GARFIELD. Since for the investigated reaction essentially only LCP fly into GARFIELD, in this experiment we discarded the GARFIELD gas stage and we operated only the CsI(Tl) crystals, which are good enough for LCP identification and energy determination. The identification energy thresholds, on average, are 3, 6, 9, and 5 MeV for  $p$ ,  $d$ ,  $t$ , and  $\alpha$  particles, respectively. Free neutrons and  $\gamma$  rays are not detected.

The  $^{12}\text{C}$  beam was provided by the XTU TANDEM, at the energy of 95 MeV with an average intensity of about 0.1 pA: it was pulsed in bunches of 2 ns width with a repetition period of 400 ns.

The  $^{13}\text{C}$  target was a self-supporting thin film, with a thickness of  $100 \mu\text{g}/\text{cm}^2$ . The target isotopic purity is known to be more than 99% at the production time. During the data taking, probably due to the vacuum level in the scattering chamber, the  $^{13}\text{C}$  foil was polluted by a certain amount of  $^{12}\text{C}$ , which is a common contaminant in vacuum systems: indeed, residual hydrocarbon molecules are reduced to graphite on the target under beam irradiation. A similar effect has been described in literature [19–21] and recently evidenced in another experiment with GARFIELD [22]. Therefore, similarly to Ref. [22], it was necessary to evaluate this background and subtract its effect from the  $^{13}\text{C}$  events.

### III. EVENT SELECTION AND $^{12}\text{C}$ BACKGROUND SUBTRACTION

Experimental results (e.g., Ref. [23]) and model calculations [24,25] show that for this type of system, fusion process accounts for more than 50% of the total reaction cross section.

The selection of fusion-evaporation events has been done via software gate, requiring the coincidence of only one “heavy” ion  $Z \geq 5$  (the evaporation residue, ER) with at least one LCP and vetoing the possible (rare) coincidences of ER with an intermediate mass fragment ( $Z = 3,4$ ). These latter cases can be ascribed to the break-up channel that is weakly populated for the excited light  $^{25}\text{Mg}$  compound nuclei. Although, these cases are interesting and have been recently studied [7] just in the context of possible  $\alpha$ -cluster effects, we neglected them in this paper. Indeed, we found a branching ratio for these break-up events of less than 1%, in agreement with the PACE4 [26–28] prediction that 99% of the  $^{25}\text{Mg}$  decays are of evaporative kind (with a final ER  $Z \geq 5$ ).

Since the projectile ions have atomic number comparable with that of ER, the chosen gate for fusion events can include some background of noncentral collisions where a quasiprojectile (QP) is detected in coincidence with some LCP. To improve the fusion event selection we also required the completeness of the detected charge: the sum of the charge of the detected fragments has to be equal to the charge of the system,  $Z_{\text{sys}}=12$ . The selected sample amounts to only 1.6% (approximately 3.3 millions) of the total sample, but it represents a high quality data set for fusion, with ER identified in  $Z$  and LCP both in  $Z$  and  $A$ , thus allowing stringent tests on the various decay chains. A final requirement has been imposed on the momentum conservation to remove residual spurious coincidence events, that are anyhow overall less than 1% within the already selected sample; they are more polluting the channels with a supposed ER in the region of the projectile ( $Z = 6 \pm 1$ ). As demonstrated in our previous article [4], the event sample selected in this way does not bias the characteristics of the totality of fusion events.

#### A. Background of reactions on $^{12}\text{C}$

To perform a detailed analysis of the various evaporation chains, we must get rid of the problem of the  $^{12}\text{C}$  contamination of the enriched  $^{13}\text{C}$  target as mentioned in Sec. II. Reactions on  $^{12}\text{C}$  ions, indeed, lead to the formation of  $^{24}\text{Mg}$ ; since we are not able to isotopically identify the ER and we do not measure neutrons, the experimental observables for the  $^{25}\text{Mg}$  decays could be biased by a spurious contribution of  $^{24}\text{Mg}$ . Moreover, we are specifically interested in searching weak differences between  $^{25}\text{Mg}$  and  $^{24}\text{Mg}$  decays, thus it is evident the need to keep under control the background and to restore a clean  $^{25}\text{Mg}$  sample of events.

To evaluate the level of spurious reactions on  $^{12}\text{C}$  nuclei, we select a specific decay channel where the contribution of the background can be easily disentangled, namely the  $6\alpha$  channel. We use the reaction  $Q$  value [5]:

$$Q = \sum_i^N E_i - E_{\text{beam}}, \quad (1)$$

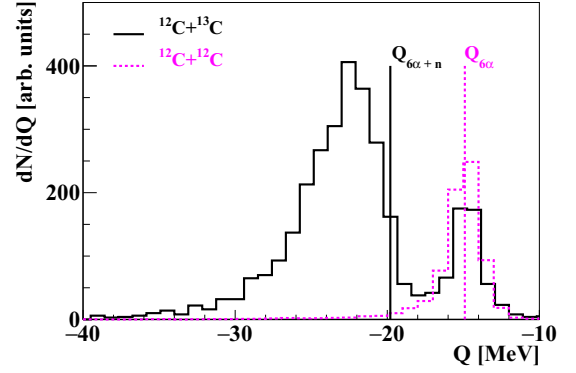


FIG. 1.  $Q$ -value distribution of complete in charge events with six detected  $\alpha$  particles. The experimental data referring to the  $^{12}\text{C}+^{13}\text{C}$  reaction are shown as a continuous black line. The  $Q$ -value distribution obtained from the  $^{12}\text{C}+^{12}\text{C}$  reaction is also shown (dashed magenta line). The vertical lines mark the expected values for the two channels  $^{24}\text{Mg} \rightarrow 6\alpha$  ( $Q_{6\alpha}$ ) and  $^{25}\text{Mg} \rightarrow 6\alpha+1n$  ( $Q_{6\alpha+n}$ ).

where  $N$  is the number of charged species,  $E_i$  is the lab. kinetic energy of the fragment  $i$  and  $E_{\text{beam}}$  is the beam energy. Exploiting the fact that  $\alpha$  clusters have not excited states close to the ground state (the first excited state is approximately at 20 MeV), we should obtain distinct  $Q$ -values associated with the disassembly of  $^{24}\text{Mg}$  in six  $\alpha$  particles or  $^{25}\text{Mg}$  in six  $\alpha$  plus one neutron (due to fusion with  $^{12}\text{C}$  or  $^{13}\text{C}$ , respectively). The spectrum obtained from the runs  $^{12}\text{C}+^{13}\text{C}$  is shown in Fig. 1 as continuous line.

In the figure we observe two distinct peaks. The main left peak is rather asymmetric and is upper limited by the value  $Q_{6\alpha+n}$  with a tail due to the missing kinetic energy of the unmeasured neutron. This is the contribution of the  $^{25}\text{Mg}$  decay. The weaker right peak is exactly centered at the value expected for  $Q_{6\alpha}$  associated with  $^{24}\text{Mg}$  decay and it is quite symmetric because no neutrons are missing. This result clearly demonstrates the presence of  $^{12}\text{C}+^{12}\text{C}$  events in the dataset. An additional confirmation comes from the  $Q$ -value distribution obtained for some specific  $^{12}\text{C}+^{12}\text{C}$  runs, purposely collected during the same experiment. The corresponding peak is drawn as a dashed (magenta) line in the same picture and perfectly matches with the right peak for the data on the  $^{13}\text{C}$  target. Moreover, no other peak is present in this case.

A quantitative estimation of the the background due to  $^{12}\text{C}+^{13}\text{C}$  can be deduced as follows. Directly from Fig. 1 we can count the number of events related to  $^{24}\text{Mg}$  decay into  $6\alpha$  ( $N_{24\text{Mg}}^{6\alpha}$ ), summing the events on the right side with respect to  $Q_{6\alpha+n}$  line. The percentage of those events is  $f = (18 \pm 1)\%$  of the total  $6\alpha$  events. This number is not the real estimation of  $^{12}\text{C}$  contribution because it does not consider the different branching ratios (BRs) for the  $^{24}\text{Mg}$  and the  $^{25}\text{Mg}$  decay into  $6\alpha$ . From the analysis of the  $^{12}\text{C}+^{12}\text{C}$  reaction presented in Refs. [4,5], we estimated that the  $^{24}\text{Mg}$  BR for  $6\alpha$  channel is  $\text{BR}_{6\alpha} = 3\%$ . So the total number of  $^{24}\text{Mg}$  events complete in charge,  $N_{24\text{Mg}}^{\text{comp}}$ , can be estimated as  $N_{24\text{Mg}}^{\text{comp}} = N_{24\text{Mg}}^{6\alpha} / \text{BR}_{6\alpha}$ . Thus, the final background level can be obtain dividing this latter by the total number of complete events  $f = N_{24\text{Mg}}^{\text{comp}} / N^{\text{comp}}$ :  $f$  results to be  $(5.8 \pm 0.5)\%$ .

With this factor, the number of spurious events of reaction on  $^{12}\text{C}$  can be estimated for (and subtracted from) each specific decay chain measured for charge-complete events. Of course, it is impossible to disentangle event by event the two reactions on  $^{12}\text{C}$  and  $^{13}\text{C}$ . Thus,  $f'$  can be used only for an average correction, although applicable to all the various decay channels. From now on, we discuss spectrum shapes and yields after removal of the  $^{12}\text{C}$  contribution. We underline that the  $^{12}\text{C}$  background subtraction comes out to be very important for the refined analyses presented in this paper, especially for the reliability of the fit procedure described in Sec. VI A.

#### IV. GENERAL CHARACTERISTICS OF FUSION REACTIONS AND COMPARISON WITH THE STATISTICAL MODEL

Before entering the detailed analysis of the individual evaporation chains, here we present some general features of the fusion event class also compared with the model predictions.

Considering the approach of this paper, it is extremely important to perform the analysis of good and selective experimental data in parallel with reliable Monte Carlo statistical codes: as done in the past, here we use two different Monte Carlo implementations of the statistical model simulations. The first one is GEMINI++ [29] and the second one is a code labeled as HF $\ell$  (*Hauser-Feshbach light*), developed by our collaboration [30,31] specifically for the study of light nuclei and described elsewhere [4]. Both codes are based on the Hauser-Feshbach theory: GEMINI++ is a general purpose code which includes several parameters, continuously refined according to experimental results. In particular, GEMINI++ contains only a smooth parametrization of the level density, whereas HF $\ell$  includes all the known single levels as found in the available databases [32]. This feature is important for the detailed investigation of the various decay channels, as we want to pursue.

For both simulations we choose, as default option, a tri-angular distribution for the angular momentum of the compound nuclei extending from zero to the maximum angular momentum for fusion ( $J_{\text{max}} = 18.5 \hbar$  calculated with the code PACE4 using the Bass model [25]). For the spin distribution we fixed a tail with a diffuseness parameter  $\Delta J = 2 \hbar$  as proposed for similar light systems [33,34] and with peaking values  $J = 15.5 \hbar$ . The shaping recipe for the spin distribution is quite similar to that of our previous paper [4] for the  $^{12}\text{C} + ^{12}\text{C}$  system. Since the spin distribution of the studied CN is not exactly known, we verified the model predictions as a function of reasonable changes in the spin values. This will be discussed afterwards but we anticipate that the conclusions are essentially unaffected by different assumptions on the spin.

The simulated events have then been filtered via a software replica of the apparatus, including the efficiencies, the resolutions and the identification thresholds of the various detectors. Of course, the same selection criteria to identify fusion events imposed on measured data have been applied as well.

In Fig. 2(a) the charge distribution for complete events is shown for the experimental and simulated events selected through the fusion gates. In the following, unless otherwise noted, HF $\ell$  and GEMINI++ results are reported in red bold and

blue thin line, respectively. We clearly observe, as expected, the bell-shaped region of the ER ( $Z \geq 5$ ) well separated from the LCP part. We remind that the absence of  $Z = 3,4$  ions is only due to the selection gate chosen for this analysis.

The overall behavior of the experimental distribution is well reproduced by both simulation codes. However, some discrepancies between experimental and simulated results appear, in particular, for the relative abundances of LCP. Both models underestimate the emission of  $Z = 2$ ; while only HF $\ell$  overestimates the emission of  $Z = 1$ . Looking at the ER region of the fragment distribution, instead, we can observe that statistical models (more HF $\ell$  than GEMINI++) nicely reproduce the yield of odd  $Z$  residues, while some disagreement is found for even charge residues (mostly  $Z = 6,8$ ). In the following it will be shown how these discrepancies, observed in detail, are related to the emission of only  $\alpha$  particles from the compound nucleus, since even- $Z$  ER can be reached through the evaporation of only  $\alpha$  particles while odd- $Z$  ER chains need the emission of at least one hydrogen ion.

Complementary information can be seen in the other panels of Fig. 2, where the angular distributions for proton and  $\alpha$  particles are shown in the laboratory frame [Figs. 2(b) and 2(c), respectively]. The angular range below  $20^\circ$  is covered by the RCO, while particles above  $30^\circ$  are detected in the GARFIELD CsI crystals. The shown angular distributions are normalized to unitary area for shape comparison. Both GEMINI++ and HF $\ell$  follow the experimental proton distribution at all emission angles. Moreover, also the angular distributions of deuterons and tritons (which altogether represent a minority fraction of 7.5% of LCP) are well reproduced by both models; they are not shown for brevity. The  $\alpha$  angular distribution, instead, shows a favored emission at more backward angles with respect to HF $\ell$ , while it is in quite good agreement with the GEMINI++ prediction. Comparing our data with those obtained for the  $^{24}\text{Mg}$  decay, the same behavior is observed as shown in Fig. 7 of Ref. [4].

As previously mentioned, the exact shape of the spin distribution of the CN is not known. On the other hand, within statistical models, the particle production rates and their phase-space properties are somewhat dependent on the assumed spin values [33,34]. Therefore, we explored how the statistical model predictions are affected by variation of the spin parameters. We run two additional calculations, assuming for both a sharp cutoff spin distribution. For the first run we put the cut-off at  $J_{\text{max}} = 15.5 \hbar$ , being aware that it would underestimate the fusion cross section; for the second set we kept the limit value of the default simulation  $J_{\text{max}} = 18.5 \hbar$  (and  $\Delta J = 0 \hbar$ )

Some differences appear for GEMINI++. In particular, the use of the lower value  $J_{\text{max}} = 15 \hbar$  decreases the  $\alpha$  emission ( $-7\%$ ), while it slightly increases the proton yield ( $+7\%$ ), thus further enlarging the differences with the experimental data. For HF $\ell$ , instead, the effects are less than 1%. The effect of zeroing the diffuseness is almost negligible, both for GEMINI++ and HF $\ell$ , increasing by only 1% the  $\alpha$  particles yield. Having proved that reasonable modifications on the spin distribution do not reduce significantly the observed discrepancies at this level of analysis, we choose the default calculations (defined at the beginning of this section) as reference and using the other

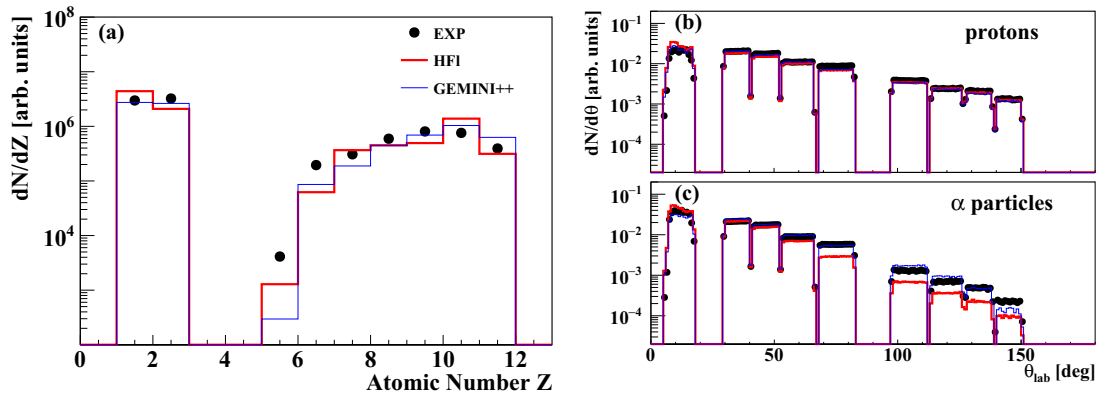


FIG. 2. (a) Charge distribution. (b, c) Proton and  $\alpha$  angular distributions in the laboratory frame. Black dots are the experimental results and the red bold and blue thin line represent the HF $\ell$  and GEMINI++ results, respectively. Both simulated charge distributions are normalized to the measured number of fusion events complete in charge, while the proton and  $\alpha$  angular distributions are normalized to unitary area for a comparison with the results in Ref. [4].

simulations to estimate the systematic uncertainties on the final results (see Sec. V).

### V. RESULTS FOR SELECTED DECAY CHANNELS

In Fig. 3 the kinetic energy distributions in the laboratory frame for protons [Figs. 3(a)–3(e)] and  $\alpha$  particles [Figs. 3(f)–3(j)] detected with GARFIELD in coincidence with ER from  $Z = 6$  up to  $Z = 10$  are shown. The collected statistics of the channel with  $Z_{\text{ER}} = 5$  is not enough for this analysis. The experimental results are indicated with filled dots while the lines are the model predictions (see caption for details). The distributions are normalized to unitary area for a easier shape comparison.

At a first sight we see that the models nicely follow the experimental data for all channels. Going into details of the various chains, for protons we observe a very good agreement between the experimental and simulated shapes, with both

models. Instead, some differences appear for  $\alpha$  particles especially for the chain ending with  $Z_{\text{ER}} = 8$  [Fig. 3(h)], where the measured high energy tail is not well reproduced by the models. There is also some disagreement in the  $\alpha$  spectra associated with  $Z_{\text{ER}} = 6, 7$  [Figs. 3(f) and 3(g), respectively], with respect to GEMINI++, while HF $\ell$  better follows the data. The simulated shapes are negligibly affected by (reasonable) changes of the parameters ruling the CN spin distribution. The good success of the statistical models makes us confident about the investigation of the further details. The discrepancies of the measured LCP multiplicities with respect to model predictions (see Sec. IV) together with the differences in the  $\alpha$  energy spectra for specific evaporation chains, are similar to the findings of Ref. [4] on  $^{24}\text{Mg}$ ; in this latter case a slight shape difference between the measured and HF $\ell$  simulated energy spectra of  $\alpha$  particles was found also for  $Z_{\text{ER}} = 6$ , not visible in the present data (Fig. 3). To explain such differences, it was argued there that  $\alpha$  emission could be favored, with respect to

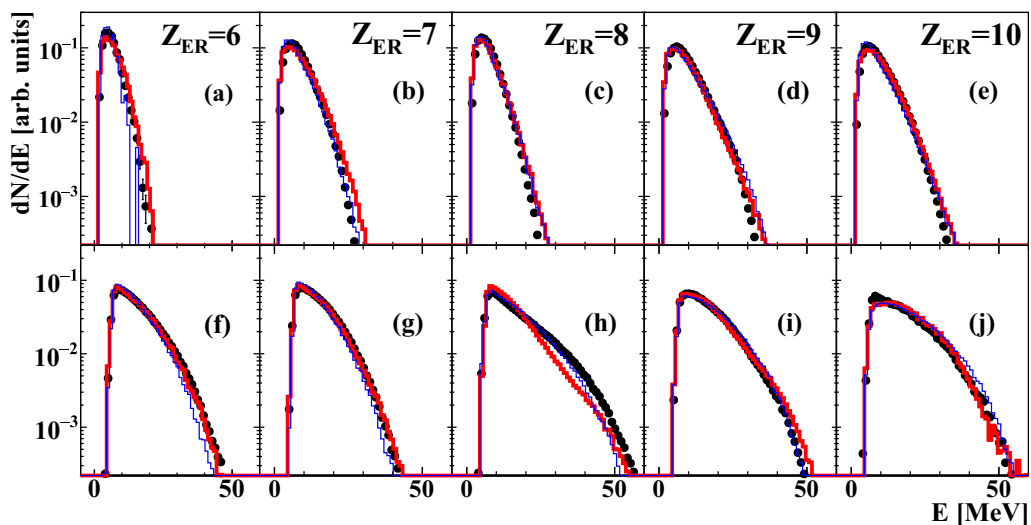


FIG. 3. Kinetic energy distributions in the laboratory frame for protons (a–e) and  $\alpha$  particles (f–j) identified in GARFIELD. Points represent experimental data, thin blue and bold red histograms represent the GEMINI++ the HF $\ell$  predictions, respectively. The distributions refer to different coincident ER, from carbon to neon, and are normalized to unitary area.

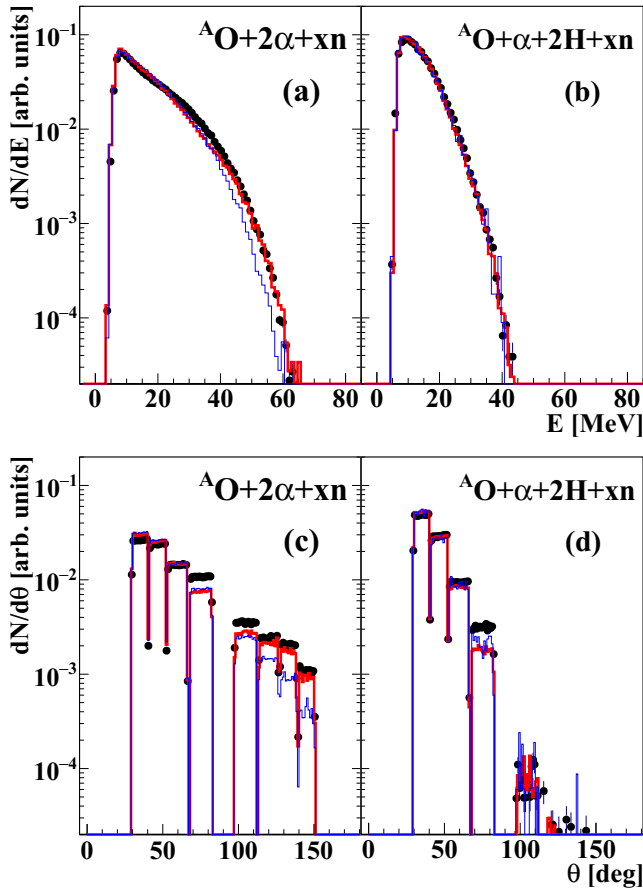


FIG. 4. Laboratory kinetic energy (a, b) and angular (c, d) distributions for  $\alpha$  particles for the channel with an oxygen ER. Experimental and simulated results are drawn according to the convention of the previous figures. The two main contributing decay channels are considered, in particular  ${}^A\text{O} + 2\alpha$  (a, c) and  ${}^A\text{O} + \alpha + 2\text{H}$  (b, d). The distributions are normalized to unitary area.

statistical models, for those channels where only  $\alpha$  particles are emitted. In turn, this could be an indication for some nonstatistical effects, not included in the Hauser-Feshbach formalism.

#### A. The case of the oxygen evaporation residues

We now focus on the oxygen channel presenting the biggest anomalies and then on the branching ratios of the channels dominated by  $\alpha$  particle emission.

In Fig. 4, the  $\alpha$  particle energy and angular distributions for the two chains  ${}^A\text{O} + 2\alpha$  [Figs. 4(a) and 4(c)] and  ${}^A\text{O} + \alpha + 2\text{H}$  (where H means  $Z = 1$ ) are shown, each normalized to unitary area. These are the two chains mainly contributing to oxygen production. The experimental and simulated data are drawn according to the already introduced convention. The results for the  ${}^A\text{O} + \alpha + 2\text{H}$  chain (right part) are fully compatible with the statistical model predictions as shape. A quite good agreement is found also for the channel  ${}^A\text{O} + 2\alpha$ , but only using the HF $\ell$  code; GEMINI++ less faithfully follows the experimental energy and angular distributions.

TABLE I. Branching ratios for relevant evaporation chains. Experimental and HF $\ell$  predictions are compared. Only the most probable chains with the largest possible  $\alpha$  multiplicities, for a fixed ER, are considered. Errors on the experimental values take into account the possible  ${}^3\text{He} + \alpha$  contamination, estimated to be around 4%. The model ranges are to consider the effect of the poor knowledge of the CN spin distribution. Statistical errors are negligible in all cases. All the values are normalized to the number of event for each  $Z_{\text{ER}}$ .

$Z_{\text{ER}}$	Channel	EXP [%]	HF $\ell$ [%]
10	${}^{21-x}\text{Ne} + xn + \alpha$	$29 \pm 1$	3.2–3.8
9	${}^{20-x}\text{F} + xn + p + \alpha$	$86 \pm 3$	84–86
8	${}^{17-x}\text{O} + xn + 2\alpha$	$69 \pm 3$	30–32
7	${}^{15-x}\text{N} + xn + p + 2\alpha$	$83 \pm 3$	90–92
6	${}^{13-x}\text{C} + xn + 3\alpha$	$97 \pm 4$	79–83

The high level of accuracy of the HF $\ell$  calculations in reproducing the phase-space of emitted LCP (over more than three orders of magnitude) demonstrates the importance of including in the model as many details as possible of the nuclear structure for the relevant nuclei. Due to this improvement of HF $\ell$  with respect to GEMINI++, in the rest of the paper we will limit the comparisons to the HF $\ell$  code only.

From Fig. 4, we can state that the kinematics of the chains ending up with an oxygen ER is accurately reproduced by a pure statistical model (HF $\ell$  code). However, since global LCP multiplicities and some inclusive  $\alpha$ -particle energy distributions (Fig. 3) show deviations with respect to the predictions, one can deduce that the weights of the various chains are not fully accounted for by the model. In other words, we must verify the quality of the model predictions as far as the BRs for the various channels are concerned, just as done in Ref. [4].

#### B. The branching ratios of the various chains

In Table I we report the BRs for the most probable chains containing the largest allowed  $\alpha$  multiplicities, for each  $Z_{\text{ER}}$ . The contributions due to the different ER isotopes, which correspond to a different number of emitted neutron ( $x$ ), are summed. Each BR is normalized to the total number of complete events with the same  $Z_{\text{ER}}$ . The errors of the experimental BRs reflect the uncertainties due to spurious  ${}^3\text{He}$  in the  $\alpha$  identification gates. The experimental BRs are compared with the HF $\ell$  results. For the model we quote ranges as fiducial limits of the BR when changing the CN spin distributions as explained in Sec. IV. Statistical errors are negligible.

The most important observation is that the model quite nicely reproduces the BRs of the chains containing an evaporated hydrogen isotope but it misses the BRs for pure  $\alpha$  emission channels (plus possible neutrons). In particular, we find that for these channels HF $\ell$  considerably underestimates the BRs with relative difference which decreases increasing  $\alpha$  multiplicity, in agreement with what observed in Ref. [4] (see Table 1 in that paper); here the effect is smaller in magnitude, except for the Ne+ $\alpha$  channel. This failure, in the case of oxygen residues, explains the differences in the  $\alpha$  energy spectrum seen

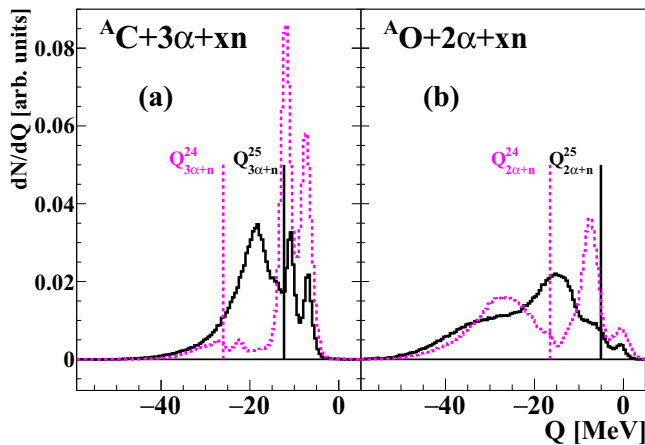


FIG. 5.  $Q$ -value distributions for the decay channel  $C + 3\alpha + xn$  (a) and  $O + 2\alpha + xn$  (b), for the  $^{25}\text{Mg}$  and  $^{24}\text{Mg}$  drawn with black continue and magenta dashed line, respectively. The vertical lines are in correspondence of the one neutron emission threshold for each system. The two distributions are shifted by the amount of the neutron separation energy  $S_n$  in  $^{25}\text{Mg}$ .

in Fig. 3, which look like the ones for the  $^{24}\text{Mg}$  (in particular, Fig. 13 of Ref. [4]).

Therefore, the additional neutron of  $^{25}\text{Mg}$  with respect to  $^{24}\text{Mg}$  seems not to strongly modify the decay paths, at least in this fusion reaction where the CN has a relatively high excitation energy: also for the  $^{25}\text{Mg}$ , indeed, the channels involving the evaporation of only  $\alpha$  particles result to be favored with respect to what predicted by a pure statistical model.

## VI. MORE REFINED COMPARISON BETWEEN THE DECAYS OF $^{25}\text{Mg}$ AND $^{24}\text{Mg}$

To further investigate the  $\alpha$  evaporation chains from excited Mg nuclei, we can directly compare the results obtained for the two fusion reactions forming  $^{24}\text{Mg}$  and  $^{25}\text{Mg}$ . This comparison is quite effective because the data have been collected with the same apparatus and with similar analysis criteria; therefore, possible systematic errors should poorly affect this comparison.

It would be very interesting to select the evaporation paths on the basis of the emitted neutron and, possibly, its emission order, for the  $^{25}\text{Mg}$ . In this respect, valuable information can be gained by the analysis of the  $Q$ -value distributions. Indeed, these distributions for  $Z$ -constrained events contain some footprints of the evaporated neutrons. In Fig. 5 we present the experimental  $Q$ -value distributions [see Eq. (1)] for the two example chains  $^A\text{C} + xn + 3\alpha$  [Fig. 5(a)] and  $^A\text{O} + xn + 2\alpha$  [Fig. 5(b)], for the two compound nuclei  $^{25}\text{Mg}$  (continuous black line) and  $^{24}\text{Mg}$  (dashed magenta line). All curves are normalized to unity. Moreover, for a better comparison, the  $^{24}\text{Mg}$  distribution has been shifted to match the  $^{24}\text{Mg}$  reaction  $Q$  value with that of  $^{25}\text{Mg}$  case (so that the ground-state values are aligned). In the pictures the vertical (continuous and dashed) lines correspond to the (one) neutron emission threshold for each system. Therefore, events on the right-hand

side of the marks are neutron less and end up at the heaviest possible ER, either in its ground or excited (but particle bound) states. In these latter cases, the  $Q$  value peaks at the energies corresponding to the emitted (and undetected)  $\gamma$  rays. Instead, in events on the left-hand side of the marks at least one neutron has been emitted. Since neutrons are undetected, the description of the low- $Q$  region of the distributions is not easy because the energy balance is incomplete; an original and more accurate analysis of these distributions will be discussed in Sec. VIA.

For the  $3\alpha$  decays, the rightmost peaks around  $-7.3$  MeV correspond to the ground state of  $^{12}\text{C}$  and  $^{13}\text{C}$ , respectively, for the  $^{24}\text{Mg}$  and  $^{25}\text{Mg}$  cases. The second peaks from the right are due to the population of the first Carbon excited states; there is a single line at 4.4 MeV ( $^{12}\text{C}$ ) for  $^{24}\text{Mg}$ , while for the  $^{25}\text{Mg}$  case we observe a mixed structure due to the three lower levels of  $^{13}\text{C}$  (3.0, 3.6, 3.9 MeV), not energetically resolved. The small peak around  $-23$  MeV visible in the  $^{24}\text{Mg}$  case is due to a spurious contribution from the channel  $^{13}\text{C} + ^3\text{He} + 2\alpha$  [5].

For the oxygen- $2\alpha$  channel (right-hand side of Fig. 5), the events ending with an oxygen in the ground state are located at  $-0.9$  MeV; for the  $^{24}\text{Mg}$  distribution the peak around  $-7$  MeV corresponds to events where  $^{16}\text{O}$  is populated in the first excited state (6 MeV). In the case of  $^{25}\text{Mg}$  no clear structures associated with excited states of  $^{17}\text{O}$  can be seen, also due to the finite energy resolution. As a general comment, we can note that for these channels, ending at carbon or oxygen residues through the emission of  $\alpha$  particles, the probability to have additional emitted neutrons is larger for the  $^{25}\text{Mg}$  than for the  $^{24}\text{Mg}$  case. Indeed, the relative yield beyond the neutron emission threshold is evidently larger for  $^{25}\text{Mg}$ . This means that in these cases, after the neutron emission the two decay paths resemble each other and, thus, reach the same ER.

To further separate the various decay chains and obtain a more stringent comparison, we now try to reconstruct also the ER mass by exploiting the shape of the  $Q$ -value distribution.

### A. Mass reconstruction in selected decay chains

As previously discussed, only below the neutron emission threshold do we know exactly the ER mass because the neutron multiplicity ( $m_n$ ) is zero. Above this threshold the shape is modeled by the kinetic energy taken by the emitted neutron; in some cases (i.e., for some specific evaporation paths) more than one neutron can be present and therefore  $Q$  extends to even lower negative values due to the larger energy deficit. Of course, for each emitted neutron, the mass of the final ER isotope is reduced by one unit. For each selected evaporation path, defined by a given ER and its accompanying LCPs, we attempted to reconstruct the isotopic population of the ER through a convolution fit of the  $Q$ -value distribution.

For the fit we need to fix some functional forms and parameters. The functional forms of the  $n$ -fold neutron emissions have been modeled on the basis of the statistical model. Indeed, here we can select chain by chain the various ER isotopes and study the shape of the  $Q$  distributions as a function of the neutron multiplicity. Basically, we adopted two different functionals for  $m_n = 0$  and  $m_n > 0$ . In the former case, we assumed a Breit-Wigner function convoluted with a Gaussian

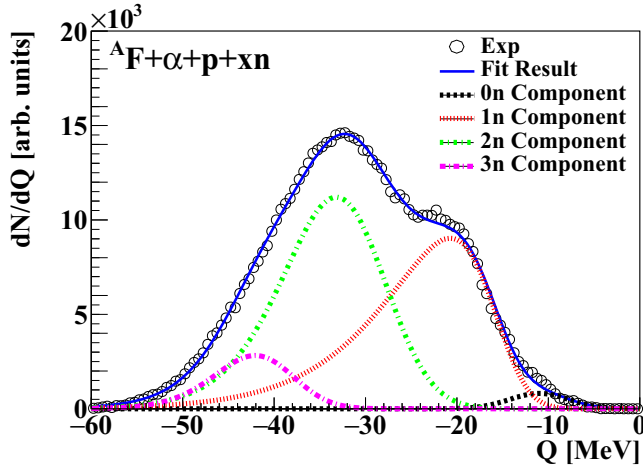


FIG. 6.  $Q$ -value experimental distribution for the  $^{25}\text{Mg} \rightarrow {}^A F + p + \alpha + xn$  chain (open dots). On the figure also the result of the fit procedure is shown (blue line), which is the sum of the various contributions related to the different neutron multiplicities represented as explained in the legend.

to keep into account the energy resolution: the initial widths are suggested by the HF $\ell$  simulation (mostly affected by experimental resolution) and centered at the known energy levels of the ER. In the case of neutron emission, each  $n$ -fold neutron contribution has the shape of the convolution of a Gaussian and a Maxwellian, whose defining parameters are tuned basing on the Monte Carlo results. The Maxwellian distributions start from the  $n$ -fold emission thresholds towards lower values of  $Q$ . The fit is applied to the measured distributions, for each type of chain constrained in ER charge and LCP. The relevant free parameters are the weights of the various  $n$ -fold neutron contributions from which we can then reconstruct the ER isotopic distributions.

Using this method we can reanalyze the chains of Table I. An example of the high quality of our fit procedure is shown in Fig. 6 for the chain  $^{25}\text{Mg} \rightarrow {}^A F + p + \alpha + xn$  path. The experimental distribution is shown (open dots) together with the fit result (blue line) which is the sum of the various components related to different neutron multiplicities, also shown in the picture. Errors have been computed varying the slope of each Maxwellian distribution by 10% around the estimated value.

The weights obtained from the fit allow to deduce the ER mass distributions. The results for  $^{25}\text{Mg}$  and  $^{24}\text{Mg}$  are compared in Fig. 7, drawn with continuous and dotted lines, respectively.

We note that the initial larger  $N/Z$  value of the source in the case of  $^{25}\text{Mg}$  brings to slightly heavier ER. Indeed, the average mass for each ER charge value is 0.3–0.4 amu larger. However the shift is lower than one amu implying that in most cases the additional neutron is not emitted as the first particle in the decay chain. We note that HF $\ell$  simulations predict average ER masses which agree with the measured ones within 20%. In particular, if the extra neutron is preferentially emitted in the first evaporation step, the detected events would correspond to the decay of a  $^{24}\text{Mg}$  source, which would explain why

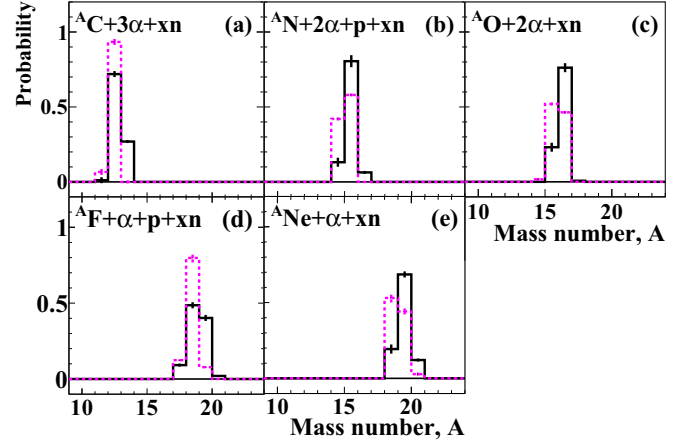


FIG. 7. Mass distributions for various ER reached in the chains Table I. The  $^{25}\text{Mg}$  (black continuous line) case is compared to the  $^{24}\text{Mg}$  case (magenta dotted line). All histograms are normalized to unitary area.

the results are similar to the ones of Ref. [4]. However, the results of Fig. 7 do not allow to discriminate between the different emission steps. Thus, we explore some other variables describing phase-space correlations among ER and emitted particles and possibly sensitive to their emission order.

## VII. EMISSION PATTERN FOR THE OXYGEN- $2\alpha$ CHANNEL

Further details on the topology of selected evaporation chains can be obtained using the Jacobi coordinates, suitable for three-body events, under the guide of the statistical model simulated data, where the particle emission order is known for each chain. As in our previous paper [5] we restrict ourselves to the specific channel oxygen- $2\alpha$  only, where the disagreement between the experimental and predicted BR is the largest; moreover, for this three-body charged decay (possibly perturbed by neutron emission) the use of the Jacobi coordinates is quite well motivated. We thus calculate the Jacobi coordinates:

$$\epsilon = \frac{E_{\alpha-\alpha}}{E_{\text{tot}}}, \quad (2)$$

$$\cos(\theta_k) = \vec{u}_O \cdot \vec{u}_{\alpha-\alpha}, \quad (3)$$

where  $E_{\alpha-\alpha}$  and  $E_{\text{tot}}$  are the relative kinetic energy between the  $\alpha$  pair and the total available energy, respectively. The Jacobi angle  $\theta_k$  is defined as the angle between the unit vector of the relative motion of the two  $\alpha$  particles  $\vec{u}_{\alpha-\alpha}$  and that of the oxygen residue momentum with respect to the  $\alpha$ - $\alpha$  center of mass. Since there are two ways of numbering the  $\alpha$  particles, for each event we calculated the Jacobi coordinates for both of them, thus forcing the cosine distribution to be symmetric around  $\cos(\theta_k) = 0$  [35]. We study the  $\alpha$ - $\alpha$  correlations when only one (undetected) neutron is emitted. Thus, for the experimental data, we limit this analysis to the events populating the  $Q$  region of Fig. 5 between the marks corresponding to  $1n$  and  $2n$  emission threshold (that is  $-20.82$  MeV). Although not

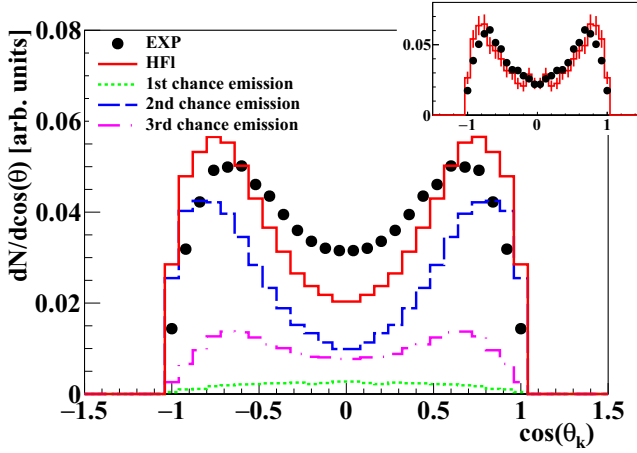


FIG. 8. Probability distribution of  $\cos(\theta_k)$  for experimental (black dots) and HF $\ell$  events of the type  $\alpha$ - $\alpha$ - $1n$ -oxygen: both distributions are normalized to unitary area. The figure also shows the various cases corresponding to the three emission orders of the neutron (see legend). The sum of these three cases gives the total HF $\ell$  curve (red continuous line). The weights are those predicted by HF $\ell$ . Each contribution is scaled by its weight to show the relative contribution to the total HF $\ell$  distribution, before and after the fit procedure. In the sub pad on the shape comparison for  $\alpha$ - $\alpha$ -oxygen events is shown.

perfect, these sharp cuts define events with oxygen ER having mass  $A = 16$ .

Since we are dealing with “false” three-body events due to the additional neutron, the relative energy  $\epsilon$  can be perturbed with respect to the original value; moreover, we observed from the Monte Carlo simulation that the relative energy  $E_{\alpha-\alpha}$  is less sensitive to the neutron emission order than the angular variable. Therefore, we focus only on this latter with the following remarks:

- (1) First-chance neutron, in the sequence  $^{25}\text{Mg}$ -neutron- $2\alpha$ ; here the  $^{24}\text{Mg}$  emits  $2\alpha$  and the construction of the angular Jacobi coordinate is not perturbed by the neutron emission;
- (2) Second-chance neutron, in the sequence  $^{25}\text{Mg}$ - $\alpha$ -neutron- $\alpha$ ; since the neutron is ejected between the  $2\alpha$  particles, both vectors in Eq. (3) are modified and a large perturbation on the decay is expected.
- (3) Third-chance neutron, in the sequence  $^{25}\text{Mg}$ - $2\alpha$ -neutron; the neutron is emitted last from an  $^{17}\text{O}$ ; thus, only  $\vec{u}_O$  is affected by the neutron emission; the perturbation is low since the  $^{16}\text{O}$  velocity is only slightly affected by the recoil, due to the large mass difference between neutron and  $^{16}\text{O}$ .

With this scheme in mind we can look at the experimental Jacobi angular distribution shown in Fig. 8 for the O- $2\alpha$  coincidences (black dots). We see that the preferred configuration is a rather aligned one with the two  $\alpha$  particles reseparating close to the direction of the recoiling ER. In the same picture also the prediction of HF $\ell$  is drawn (red bold line); here we can exactly choose the chain leading to  $^{16}\text{O}$  residues. We see that the model overestimates the aligned configurations. Before going into further detail, it is important to check the capability

TABLE II. Weights for the first-second-third chance emission of the neutron in the evaporation chains of  $^{25}\text{Mg}$  to O+ $\alpha$ + $\alpha$ . The left column reports the original weights predicted by HF $\ell$ , while the right one lists the weights obtained through the fit procedure explained in the text. Errors are only statistical and calculated from the  $\chi^2$  distribution of the fit procedure.

	HF $\ell$ original code	HF $\ell$ after fit
First chance $n$	5%	$20 \pm 2\%$
Second chance $n$	70%	$20 \pm 2\%$
Third chance $n$	25%	$60 \pm 4\%$

of HF $\ell$  to properly reproduce the shape of the Jacobi angular distributions. This has been done using the O+ $2\alpha$  events without neutron, selected as those below the neutron threshold (right side of the mark in Fig. 5). The result for this case is drawn in the inset of Fig. 8. Within the limits of the statistics we observe a noticeable agreement between experiment and model that can be used as a guide for a further investigation of the Jacobi coordinate for the O+ $2\alpha$ + $1n$  events.

We start separating the cases of the three emission orders to explore how the  $\cos(\theta_k)$  distribution changes from one to another. The three contributions to the total spectrum are shown in Fig. 8; the corresponding relative weights are reported in the left column of Table II. Clearly, the second-chance emission dominates while the first chance is a minority case. Moreover, we see that the first-chance neutron case is the only one capable of filling the region  $\cos(\theta_k) \approx 0$  because the corresponding shape is almost flat with a broad bump at zero. The other two cases, instead, tend to populate more aligned configurations. Probably when the neutron is first-chance, it has on average high energy and the following two (relatively slow)  $\alpha$  produce a moderate recoil on the heavier partner. Instead, if an  $\alpha$  particle is emitted first, it has high energy (on average) and the kick given the residue favors polarized configurations [ $\cos(\theta_k) \approx \pm 1$ ].

Using the shapes predicted by the model, we estimated the new weights of the three cases corresponding to the three emission orders via a fit procedure on the experimental result. Specifically, we looked for the minimum of a purposely defined  $\chi^2$  variable as follows:

$$\chi^2 = \sum_{i=0}^N \frac{[h_{\text{exp}}(i) - h_{\text{HF}\ell}(i)]^2}{\sigma_{\text{exp}}^2(i)}, \quad (4)$$

with

$$h_{\text{HF}\ell} = w_1 h_{\text{first}} + w_2 h_{\text{second}} + w_3 h_{\text{third}}, \quad (5)$$

where  $h_{\text{exp}}(i)$  and  $h_{\text{HF}\ell}(i)$  are the values of the experimental and simulated spectra at the  $i$ th bin, respectively; the experimental variance for the  $i$ th bin,  $\sigma_{\text{exp}}^2(i)$ , is obtained assuming a Poisson distribution on the counts registered in the bins;  $h_{\text{HF}\ell}$  is the total model distribution composed by the three cases with weights  $w_1$ ,  $w_2$ , and  $w_3$ , which are the fit parameters. The statistics of the simulated events is such that the errors on the model distributions are negligible. The new fitted weights are listed in the right column of Table II and the high quality of the result

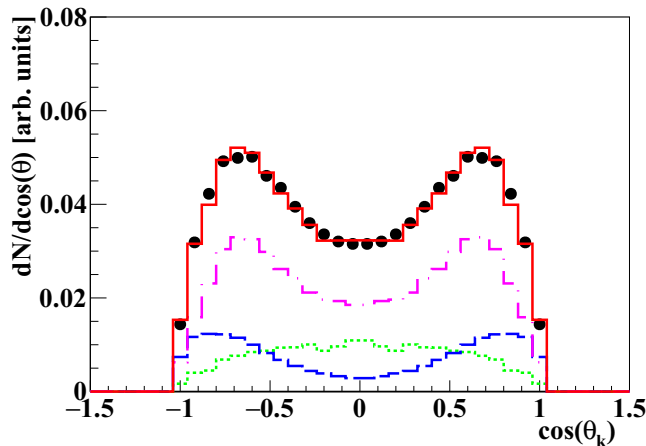


FIG. 9. Same as described in the caption of Fig. 8 but with the weights assigned through the fit procedure explained in the text.

is shown in Fig. 9, where the three contributions are scaled by the new weights; the summed curve nicely matches with the experimental finding.

We can conclude that the experimental data suggest a preferred  $\alpha$ - $\alpha$ - $n$  emission as already found for the same kind of decays from  $^{24}\text{Mg}$  [5]. On the other side, the fit indicates that the neutron first chance emission is much more probable than predicted by the statistical model. In these cases, after removing the neutron, the emission path from the decay of  $^{25}\text{Mg}$  becomes almost identical to that of  $^{24}\text{Mg}$  and this situation is underestimated by HF $\ell$  calculations. The fact that the evaporation chains of  $^{24}\text{Mg}$  and  $^{25}\text{Mg}$  are similar when the excess neutron is promptly removed along the evaporation path could partially explain the similarity between the decays of the two Mg nuclei and the persistence of the differences found between the experimental and simulated data.

Even more interesting: we can observe a preferential occurrence of chains where two  $\alpha$  are emitted one after the other. In fact, the cases with first- or third chance  $n$ -emission are experimentally much more probable than predicted by the HF $\ell$  code, which instead favors  $\alpha$ - $n$ - $\alpha$  chains. This finding could again hint to some  $\alpha$ -cluster structure developing during the path to fusion, of course, not included in our model. It is very remarkable, in this direction, the message proposed in a theoretical paper recently published [36]. There, in the context of refined TDHF calculations, the authors show that  $\alpha$ -clustered configurations occur during the precompound phases in fusion reactions of light heavy-ions (either with  $N = Z$  or with small neutron excess) above the barrier. Another interesting possibility could be the persistence in nuclei at high excitation energy and with small neutron excess, of the linear O- $\alpha$ - $\alpha$  chain theoretically predicted in the excited spectrum of  $^{24}\text{Mg}$  [37,38]. These two interpretations represent promising theoretical directions for further understanding of the effects presented in this paper.

## VIII. CONCLUSIONS

We have described the experimental results of an experiment on  $^{12}\text{C} + ^{13}\text{C}$  fusion reactions at 95 MeV bombarding

energy, performed with the apparatus GARFIELD+RCO at the INFN Laboratori Nazionali di Legnaro (Italy). Motivated by the recent interest in the investigation of the interplay of nuclear structure and reaction mechanisms in light systems and in continuation with our previous studies [4,5], we focused on the decay of the hot  $^{25}\text{Mg}$  compound nucleus and we studied the properties of its various decay chains. Specifically, the objective was to verify if the disagreement of some observables with respect to refined statistical model calculations found for the decay of the autoconjugate  $^{24}\text{Mg}$  nucleus persist also with the addition of one neutron.

Thanks to the large efficiency and the good identification capability of the detectors, we could precisely select and study the various fusion-evaporation chains, strongly constrained by the request of total charge conservation. Furthermore, an original attempt was also done to reconstruct the mass of the evaporation residues even without measuring emitted neutrons, by exploiting the  $Q$ -value distribution for selected channels and using our refined Hauser-Feshbach calculations to model the various contributions.

The main results are the following. Similar to previous works, most fusion-evaporation features are well accounted for by a refined version of the statistical model. Still, some disagreements have been found when looking at the details of specific evaporation chains, mainly those dominated by the emission of  $\alpha$  particles and reaching even- $Z$  ER. In particular, as for the  $^{24}\text{Mg}$  case, a clear mismatch between experimental and predicted BR was found for the channels ending up with  $Z_{\text{ER}} = 6, 8, 10$ , reached via pure  $\alpha$  emissions. The model strongly underpredicts these channels. The analogy of this result with the previous findings on  $^{24}\text{Mg}$  [4] suggests that the excess neutron in  $^{25}\text{Mg}$  does not considerably modify the evaporation paths and that possible  $\alpha$ -cluster effects still persist in fusion reactions, not being washed out by the additional neutron. This is suggested by an analysis in terms of the Jacobi angular coordinate, applied to the selected decay O+ $2\alpha$ + $n$ . The deduced tendency of the  $\alpha$  particles to be preferentially emitted one after the other and not separated by neutron emission (as predicted by the model) supports the argument.

Further, even more selective experiments would be necessary to better disentangle specific evaporation chains. More severe constraints on the decay chains could be imposed by the coincident detection of neutrons but this is a very challenging effort presently not yet at hand. Alternatively, efforts can be made to improve the isotopic identification capability of the ER detectors to select mass resolved decay chains, event by event. The original attempt done in this paper to deduce the ER masses goes in this direction but it is not apt to describe the mass balance for every event. Improvements of the isotopic separation capability of detectors are in progress in our collaboration and the recent developments are promising to reach even  $A$  identification for residues with the RCO telescopes, at least for light nuclei, like those studied in this paper. Of course, the experimental improvements should be accompanied by more refined theoretical calculations, able to go beyond the Hauser-Feshbach scheme and including effects related to cluster or resonance states. The recent theoretical paper [36] is very suggestive, showing, in the framework of time-dependent HF calculations, the formation of deformed

$\alpha$ -cluster configurations during the path to fusion in light heavy-ion collisions above the barrier.

### ACKNOWLEDGMENTS

Thanks are due to the accelerator staff of Legnaro Laboratories for having provided good-quality beams and to

the Target Lab of INFN-LNL and INFN-LNS for providing the targets used during this experiment. This work was partially supported by grants from the Italian Ministry of Education, University, and Research under Contract PRIN 2010-2011. We also thank Prof. G. Poggi for very helpful suggestions.

- 
- [1] B. Heusch, C. Beck, J. P. Coffin, R. M. Freeman, A. Gallmann, F. Haas, F. Rami, P. Wagner, and D. E. Alburger, *Phys. Rev. C* **23**, 1527 (1981).
- [2] W. M. Oertzen, *Clusters in Nuclei*, Lecture Notes in Physics Vol. 1 (Springer-Verlag, Berlin, 2011).
- [3] Y. Funaki, *Phys. Rev. C* **97**, 021304 (2018).
- [4] L. Morelli, G. Baiocco, M. D'Agostino, F. Gulminelli, M. Bruno, U. Abbondanno, S. Appannababu, S. Barlini, M. Bini, G. Casini *et al.*, *J. Phys. G: Nucl. Part. Phys.* **41**, 075107 (2014).
- [5] L. Morelli, G. Baiocco, M. D'Agostino, F. Gulminelli, M. Bruno, U. Abbondanno, S. Appannababu, S. Barlini, M. Bini, G. Casini *et al.*, *J. Phys. G: Nucl. Part. Phys.* **41**, 075108 (2014).
- [6] J. Vadas, T. K. Steinbach, J. Schmidt, V. Singh, C. Haycraft, S. Hudan, R. T. deSouza, L. T. Baby, S. A. Kuvin, and I. Wiedenhöver, *Phys. Rev. C* **92**, 064610 (2015).
- [7] S. Manna, T. K. Rana, C. Bhattacharya, S. Bhattacharya, S. Kundu, K. Banerjee, P. Roy, R. Pandey, V. Srivastava, A. Chaudhuri *et al.*, *Phys. Rev. C* **94**, 051601 (2016).
- [8] C. Beck, *J. Phys.: Conf. Ser.* **569**, 012002 (2014).
- [9] L. Morelli, M. Bruno, M. D'Agostino, G. Baiocco, F. Gulminelli, U. Abbondanno, S. Barlini, M. Bini, G. Casini, M. Cinausero *et al.*, *J. Phys. G: Nucl. Part. Phys.* **43**, 045110 (2016).
- [10] L. Morelli, M. Bruno, M. D'Agostino, G. Baiocco, F. Gulminelli, M. Cinausero, M. Degerlier, D. Fabris, F. Gramegna, T. Marchi *et al.*, *EPJ Web Conf.* **122**, 11002 (2016).
- [11] Ad. R. Raduta, B. Borderie, E. Geraci, N. Le Neindre, P. Napolitani, M. F. Rivet, R. Alba, F. Amorini, G. Cardella, M. Chatterjee *et al.*, *Phys. Lett. B* **705**, 65 (2011).
- [12] L. Quattrocchi, L. Acosta, F. Amorini, A. Anzalone, L. Auditore, I. Berceanu, G. Cardella, A. Chbihi, E. De Filippo, D. Dell'Aquila *et al.*, *EPJ Web Conf.* **117**, 07020 (2016).
- [13] M. Kaur, B. Singh, S. K. Patra, and R. K. Gupta, *Phys. Rev. C* **95**, 014611 (2017).
- [14] B. Borderie, Ad. R. Raduta, G. Ademard, M. F. Rivet, E. De Filippo, E. Geraci, N. Le Neindre, R. Alba, F. Amorini, G. Cardella *et al.*, *Phys. Lett. B* **755**, 475 (2016).
- [15] K. Schmidt, X. Cao, E. J. Kim, K. Hagel, M. Barbui, J. Gauthier, S. Wuenschel, G. Giuliani, M. R. D. Rodrigues, H. Zheng *et al.*, *Phys. Rev. C* **95**, 054618 (2017).
- [16] D. Dell'Aquila, I. Lombardo, G. Verde, M. Vigilante, L. Acosta, C. Agodi, F. Cappuzzello, D. Carbone, M. Cavallaro, Cherubini *et al.*, *Phys. Rev. Lett.* **119**, 132501 (2017).
- [17] L. Morelli, G. Baiocco, M. D'Agostino, M. Bruno, F. Gulminelli, M. Cinausero, M. Degerlier, D. Fabris, F. Gramegna, T. Marchi *et al.*, *EPJ Web Conf.* **66**, 03064 (2014).
- [18] M. Bruno, F. Gramegna, T. Marchi, L. Morelli, G. Pasquali, G. Casini, U. Abbondanno, G. Baiocco, L. Bardelli, S. Barlini *et al.*, *Eur. Phys. J. A* **49**, 128 (2013).
- [19] C. T. Papadopoulos, R. Vlastou, E. N. Gazis, P. A. Assimakopoulos, C. A. Kalfas, S. Kossionides, and A. C. Xenoulis, *Phys. Rev. C* **34**, 196 (1986).
- [20] R. A. Dayras, R. G. Stokstad, Z. E. Switkowski, and R. M. Wieland, *Nucl. Phys. A* **265**, 153 (1976).
- [21] D. G. Kovar, D. F. Geesaman, T. H. Braid, Y. Eisen, W. Henning, T. R. Ophel, M. Paul, K. E. Rehm, S. J. Sanders, P. Sperr *et al.*, *Phys. Rev. C* **20**, 1305 (1979).
- [22] S. Piantelli, S. Valdré, S. Barlini, G. Casini, M. Colonna, G. Baiocco, M. Bini, M. Bruno, A. Camaiani *et al.*, *Phys. Rev. C* **96**, 034622 (2017).
- [23] M. E. Ortiz, J. G. del Campo, Y. D. Chan, D. E. DiGregorio, J. L. C. Ford, D. Shapira, R. G. Stokstad, J. P. F. Sellschop, R. L. Parks, and D. Weiser, *Phys. Rev. C* **25**, 1436 (1982).
- [24] S. K. Gupta and S. Kailas, *Z. Phys. A: At. Nucl.* **317**, 75 (1984).
- [25] R. Bass, *Nucl. Phys. A* **231**, 45 (1974).
- [26] A. Gavron, *Phys. Rev. C* **21**, 230 (1980).
- [27] <http://lise.nslc.msu.edu/pace4.html>.
- [28] O. B. Tarasov and D. Bazin, *Nucl. Instrum. Methods Phys. Res., Sect. B* **266**, 4657 (2008).
- [29] R. J. Charity, *Phys. Rev. C* **82**, 014610 (2010).
- [30] G. Baiocco, Ph.D. thesis, Università di Bologna and Université de Caen Basse-Normandie, 2010, <http://amsdottorato.cib.unibo.it/4295>.
- [31] G. Baiocco, L. Morelli, F. Gulminelli, M. D'Agostino, M. Bruno, U. Abbondanno, S. Barlini, M. Bini, S. Carboni, G. Casini *et al.*, *Phys. Rev. C* **87**, 054614 (2013).
- [32] [www.nndc.bnl.gov/nudat2/](http://www.nndc.bnl.gov/nudat2/).
- [33] A. Dey, S. Bhattacharya, C. Bhattacharya, K. Banerjee, T. K. Rana, S. Kundu, S. R. Banerjee, S. Mukhopadhyay, D. Gupta, and R. Saha, *Eur. Phys. J. A* **41**, 39 (2009).
- [34] D. Mahboub, C. Beck, B. Djerroud, R. M. Freeman, F. Haas, R. Nouicer, M. Rousseau, P. Papka, A. Sánchez i Zafra, S. Cavallaro *et al.*, *Phys. Rev. C* **69**, 034616 (2004).
- [35] L. V. Grigorenko, T. D. Wiser, K. Mercurio, R. J. Charity, R. Shane, L. G. Sobotka, J. M. Elson, A. H. Wuosmaa, A. Banu, M. McCleskey, L. Trache *et al.*, *Phys. Rev. C* **80**, 034602 (2009).
- [36] B. Schuetrumpf and W. Nazarewicz, *Phys. Rev. C* **96**, 064608 (2017).
- [37] M. Girod and P. Schuck, *Phys. Rev. Lett.* **111**, 132503 (2013).
- [38] T. Ichikawa, J. A. Maruhn, N. Itagaki, K. Matsuyanagi, P.-G. Reinhard, and S. Ohkubo, *Phys. Rev. Lett.* **109**, 232503 (2012).